

## Application of a newly developed software program for image quality assessment in cone-beam computed tomography

Marcus Vinicius Linhares de Oliveira<sup>1,2,\*</sup>, António Carvalho Santos<sup>3</sup>, Graciano Paulo<sup>4</sup>, Paulo Sergio Flores Campos<sup>2</sup>, Joana Santos<sup>4</sup>

<sup>1</sup>Department of Health Technology and Biology, Federal Institute of Bahia, Salvador, BA, Brazil

<sup>2</sup>Department of Interactive Processes of Organs and Systems, Institute of Health Sciences, Federal University of Bahia, Salvador, BA, Brazil

<sup>3</sup>Department of Complementary Sciences, Coimbra Health School, Polytechnic Institute of Coimbra, Portugal

<sup>4</sup>Department of Medical Imaging and Radiotherapy, Coimbra Health School, Polytechnic Institute of Coimbra, Portugal

### ABSTRACT

**Purpose:** The purpose of this study was to apply a newly developed free software program, at low cost and with minimal time, to evaluate the quality of dental and maxillofacial cone-beam computed tomography (CBCT) images.

**Materials and Methods:** A polymethyl methacrylate (PMMA) phantom, CQP-IFBA, was scanned in 3 CBCT units with 7 protocols. A macro program was developed, using the free software ImageJ, to automatically evaluate the image quality parameters. The image quality evaluation was based on 8 parameters: uniformity, the signal-to-noise ratio (SNR), noise, the contrast-to-noise ratio (CNR), spatial resolution, the artifact index, geometric accuracy, and low-contrast resolution.

**Results:** The image uniformity and noise depended on the protocol that was applied. Regarding the CNR, high-density structures were more sensitive to the effect of scanning parameters. There were no significant differences between SNR and CNR in centered and peripheral objects. The geometric accuracy assessment showed that all the distance measurements were lower than the real values. Low-contrast resolution was influenced by the scanning parameters, and the 1-mm rod present in the phantom was not depicted in any of the 3 CBCT units. Smaller voxel sizes presented higher spatial resolution. There were no significant differences among the protocols regarding artifact presence.

**Conclusion:** This software package provided a fast, low-cost, and feasible method for the evaluation of image quality parameters in CBCT. (*Imaging Sci Dent* 2017; 47: 75-86)

**KEY WORDS:** Image Quality; Cone-Beam Computed Tomography; Quality Control; Quality Assurance

### Introduction

Cone-beam computed tomography (CBCT) examinations have become significantly more common in recent years. Currently, CBCT is widely used in oral surgery, maxillofacial surgery, temporomandibular joint studies, orthodontics, endodontics, and periodontics.<sup>1-3</sup> The most common clinical reason for a CBCT examination is the decision to place an oral implant. Even CBCT units with

relatively low radiation doses are still considered higher-dose modalities than other radiographic dental imaging methods.<sup>4</sup> One of the factors related to this is the lack of standardization in the CBCT equipment used in terms of configuration options. The combinations of different exposure parameters, such as tube voltage, field of view (FOV), and angle of rotation,<sup>5,6</sup> directly influence the radiation dose values and image quality.<sup>7</sup> Despite these differences in CBCT equipment, the obtained images must have high diagnostic quality, especially in periodontics and endodontics, where small details must be analyzed.<sup>8</sup>

Recently, comprehensive guidelines based on evidence acquired from the usage of CBCT in dentistry were pub-

Received August 26, 2016; Revised March 1, 2017; Accepted April 24, 2017

\*Correspondence to : Dr. Marcus Vinicius Linhares de Oliveira

Department of Health Technology and Biology, Federal Institute of Bahia, R. Emídio dos Santos, SN - Barbalho, Salvador - BA, Brazil, 40301-015.

(Tel) 55-71-2102-9412, (Fax) 55-71-2102-9451, (E-mail) [marcusradiology@gmail.com](mailto:marcusradiology@gmail.com)

Copyright © 2017 by Korean Academy of Oral and Maxillofacial Radiology

This is an Open Access article distributed under the terms of the Creative Commons Attribution Non-Commercial License (<http://creativecommons.org/licenses/by-nc/3.0>) which permits unrestricted non-commercial use, distribution, and reproduction in any medium, provided the original work is properly cited.

Imaging Science in Dentistry · pISSN 2233-7822 eISSN 2233-7830

lished in the European Commission Radiation Protection Report No. 172.<sup>9</sup> These guidelines include quality assurance and optimization strategies to ensure CBCT best practices. The establishment of quality assurance testing is important to ensure diagnostic information maintenance using optimized protocols. Moreover, the radiation doses must be as low as reasonably achievable. In addition, the aspects of the imaging process, including objective measures of equipment performance, patient dosimetry, and evaluation of clinical image quality, should be included in the tests.<sup>10,11</sup> The American Academy of Oral and Maxillofacial Radiology (AAOMR)<sup>12</sup> also proposed recommendations related to the use of CBCT; however, they did not provide clear evaluation parameters. In the AAOMR recommendations, it is stated that the quality assurance program should include documentation of the performed quality control tests, a record of equipment performance monitoring results, dosimetry results, and a chart of patient- and task-specific exposure parameters.

System quality control should not be performed based on subjective image evaluations because depending on the computer graphics card, images can be displayed with misrepresentations of the grayscale levels. Likewise, imperfect interpolation algorithms may lead to truncation or round-off errors. In other words, subjective evaluation may contribute to many confounding factors that affect the obtained results.<sup>13</sup>

The use of phantoms is essential to make measurements of image quality parameters. Furthermore, automatic image evaluation is suggested to avoid interobserver and intraobserver disagreement.<sup>9</sup> Few studies have presented software to assess image quality in CBCT. The procedures for determining image quality parameters presented in some software programs are manual, very time-consuming, and for the most part very expensive.<sup>13-15</sup> Consequently, this type of evaluation discourages the use of quantitative CBCT parameter analysis in clinical practice.

Therefore, the purpose of this study was to develop a package for automatic quality control, with dedicated open-access software and a quality control informatics system, that could be used to evaluate the quality of CBCT images and to manage a CBCT system over time.

### Materials and Methods

This study was divided into 3 phases: creation of a quality control phantom, the development of dedicated software for that phantom, and the development of an application to perform record management and data quality

control. After phantom development, CBCT images were acquired to collect data to use in the development of dedicated software for the phantom. The structure of the study is presented in Figure 1.

#### Quality control phantom

A phantom model, referred to as CQP-IFBA, was created in polymethyl methacrylate (PMMA) based on the CQ-01-IFBA prototype developed by Dr. Wilson Batista. This cylindrical phantom, 70 mm high and 150 mm in diameter, is of modular design and divided into 7 circular discs of PMMA (10 mm high and 140 mm in diameter). The phantom consists of different materials that represent structures with various densities, allowing image quality parameters to be evaluated. The phantom structure was elaborated according to the image quality parameters, as presented in Table 1.

To ensure that disc rotation did not occur, black disc marks were performed with a radiotransparent material (Fig. 2A). A docking slot was created in all the small discs disposed inside the regular discs to avoid disc rotation (Fig. 2B). Two black vertical landmarks were also defined to ensure that the phantom was aligned according to the CBCT laser positioners, since for optimal performance, it is essential to correctly position the phantom.

At the bottom of the phantom, disc 1 allowed the evaluation of geometric accuracy via the measurement of distances between the micro-holes. Disc 2 was a homogeneous PMMA disc (without drilling or landmarks), used to evaluate the image noise and uniformity. Disc 3 had a hole with air placed in the center of the PMMA disc. Further, disc 4 contained 5 elements with different densities

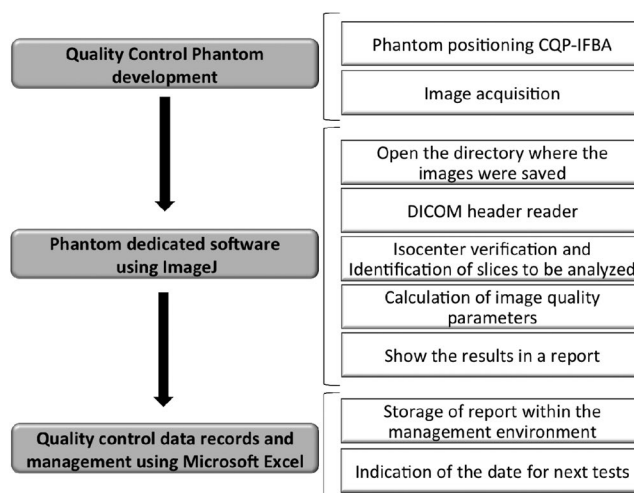
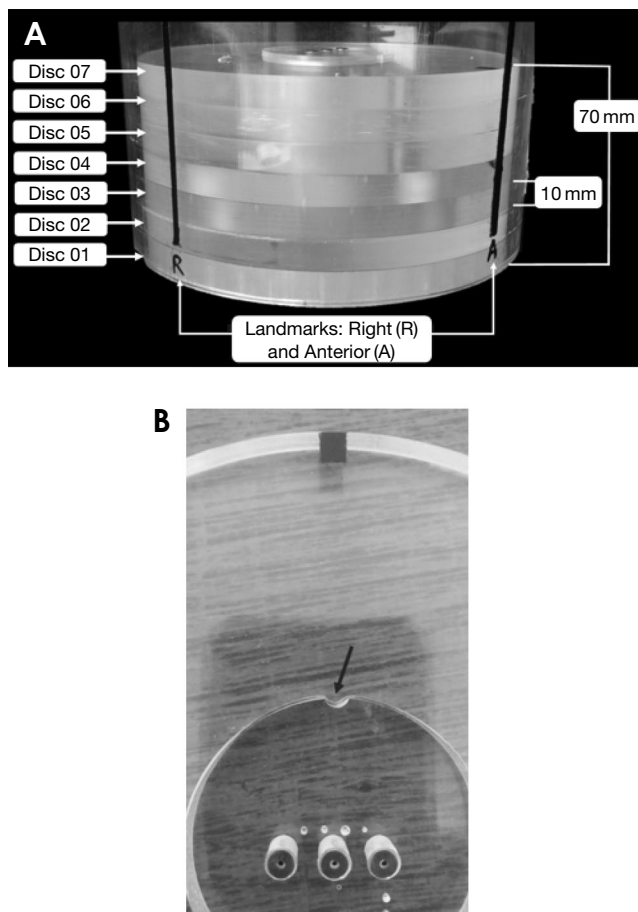


Fig. 1. Structure of study

**Table 1.** Image quality parameters and structure of phantom CQP-IFBA

Image quality parameters	Structure of phantom	Disc ID
Geometric accuracy	PMMA disc containing micro holes ( $\varnothing$ 1 mm) with 10 mm in distance between them.	01
Uniformity	Homogeneous PMMA Disc	02
Signal to noise ratio	6 elements with various densities (PTFE, PP, nylon, Delrin, PVC, Air, PMMA)	03/04
Noise	Homogeneous PMMA Disc	02
Contrast to noise ratio	6 elements with various densities (PTFE, PP, PVC, nylon, Delrin, Air, PMMA)	03/04
Spatial resolution	Bar pattern	05
Low contrast	Seven rods of PP with $\varnothing$ 7 mm, $\varnothing$ 6 mm, $\varnothing$ 5 mm, $\varnothing$ 4 mm, $\varnothing$ 3 mm, $\varnothing$ 2 mm, $\varnothing$ 1 mm and 10 mm in height.	06
Artifact	Three titanium rods in parallel	07

PMMA: polymethyl methacrylate, PTFE: polytetrafluoroethylene, PP: polypropylene, PVC: polyvinyl chloride



**Fig. 2.** Design of the phantom CQP-IFBA. A. Seven discs and location landmarks, B. docking slot inside the regular discs

placed in the periphery and the center of the disc: polyvinylchloride (PVC), polytetrafluoroethylene (PTFE), nylon, Delrin (polyoxymethylene), and polypropylene (PP). The rods inserted were 15 mm in diameter and 10 mm high. Both discs 3 and 4 were used to assess the contrast-to-noise ratio (CNR) and the signal-to-noise ratio (SNR). However, when the exposure protocol or CBCT unit had

a small FOV ( $\leq 100$  mm), only the centered rods were used. Disc 5 allowed the evaluation of the spatial resolution (5 line pairs/cm [lp/cm] to 16 lp/cm) by the bar pattern. Low-contrast assessment was evaluated with disc 6. In this disc, 7 rods of PP with diameters of 7 mm, 6 mm, 5 mm, 4 mm, 3 mm, 2 mm, and 1 mm, all 10 mm high, were inserted into the PMMA disc. In the upper part of the phantom, disc 7 was used to evaluate the artifact index. This final disc had a small disc inserted (50 mm in diameter and 10 mm in height) with 3 titanium implants (5 mm in diameter and 10 mm in height) to produce the metallic artifacts. The implants were located in the same plane and in parallel.

CBCT phantom acquisition was performed using 3 different CBCT scanners: NewTom<sup>TM</sup> 5G (QR srl, Verona, Italy), Cranex<sup>®</sup> 3D (Soredex Oy, Tuusula, Finland), and Scanora 3D (Soredex Oy, Tuusula, Finland). The experimental tests were conducted according to the exposure parameters available in each device, with current and optimized protocols.

To ensure that the phantom was correctly positioned within the FOV, before the phantom acquisitions, a scouting view was performed. A single scan was sufficient to include the whole phantom. The images were exported and viewed using ImageJ version 1.49e (National Institutes of Health, Bethesda, MD, USA).

#### Phantom-dedicated software

The CBCT quality assurance (QA) software was developed on ImageJ (National Institutes of Health, USA), to analyze image quality. After the phantom image acquisitions, Digital Imaging and Communication on Medicine (DICOM) images were opened in the ImageJ software and the user identified the directory where the images were saved. The DICOM header was read to identify the manufacture, the number of images, the voxel size (mm), FOV (mm), tube voltage (kV), tube current (mAs), expo-

sure time (ms), and dose area product ( $\text{mGy} \cdot \text{cm}^2$ ). Information from the equipment manufacturer indicated the image acquisition range orientation (top to bottom, or bottom to top).

After this procedure, the macro created an 80-mm circular region of interest (ROI) in all the image centers to identify the highest standard deviation pixel value, which corresponded to disc 03, which had a hole inside, with the air corresponding to the lowest pixel value. Based on the automatic image selection of disc 03, the positioning of the phantom was verified based on a square ROI; that is, analyzed using rectangular vertical and horizontal ROIs to identify the greatest standard deviation. The square ROI definition was based on the central part of the phantom, considering the vertical number of pixels, divided by 3 (Fig. 3).

If the phantom was not well positioned according to the isocenter, the position of the ROI was automatically corrected in the image. Based on the result of the maximum standard deviation of the ROI, the center of the image was identified by its coordinates in the x- and y-axes. Thus, this automatic process reduced variability due to the lack of operator skill or the observer's experience in handling of the phantom. After the identification of disc 3, the best image per disc was selected in the order presented in Table 2.

An image for each of the 7 discs was selected, meaning

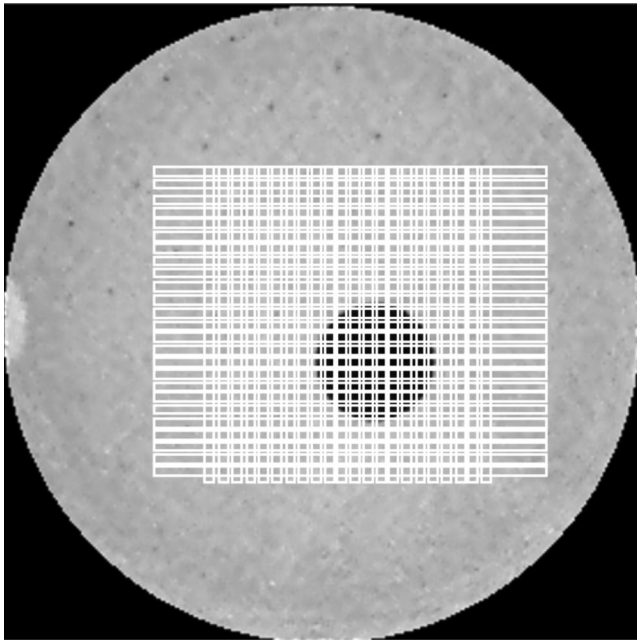


**Fig. 3.** Rectangular ROIs (vertical and horizontal) are drawn to identify highest standard deviation on disc 3.

that 7 images were evaluated in total. The ROIs used for image quality analyses were created in the same points of interest in the phantom based on the matrix and voxel size previously detected on the DICOM header. This allowed the software to be adapted to different manufacturers.

ROIs for image quality analysis were automatically defined based on image coordinates from the known distances of structures on the phantom. The image quality parameters evaluated were: SNR, CNR, image uniformity, image noise, geometric accuracy, spatial resolution, low-contrast resolution, and the artifact index. The methods are described below.

To evaluate the SNR, 6 circular ROIs (diameter, 8 mm) were placed in 6 elements of different densities: PTFE, PP, nylon, Delrin, air, and PMMA. These elements represented the signal response of different structures. The macro obtained the SNR values as:

$$\text{SNR} = \frac{\text{Mean value of pixels}}{\text{Standard deviation}} \quad (1)$$

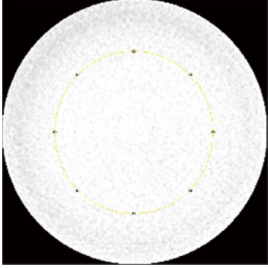
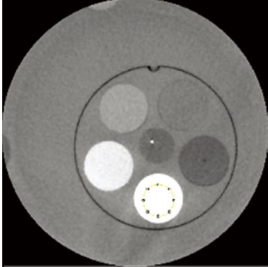
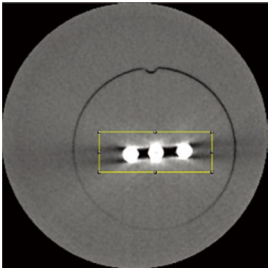
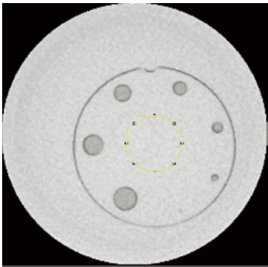
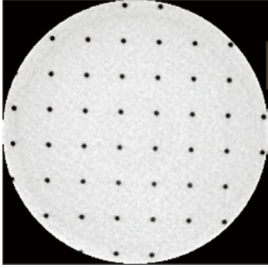
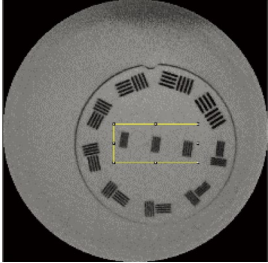
The CNR was evaluated using PTFE, PP, nylon, Delrin, air, and PMMA. A circular ROI (diameter, 8 mm) was drawn in the center of each material. For FOVs smaller than 100 mm in diameter, only the centered objects placed in disc 4 were evaluated. However, the air was evaluated using disc 03. The CNR value was calculated as:

$$\text{CNR} = \frac{\text{Signal}_{\text{material}} - \text{Signal}_{\text{PMMA}}}{\frac{\text{SD}_{\text{Material}} + \text{SD}_{\text{PMMA}}}{2}} \quad (2)$$

where  $\text{Signal}_{\text{material}}$  is the mean pixel value of the material;  $\text{Signal}_{\text{PMMA}}$  is the mean pixel value of the background (PMMA),  $\text{SD}_{\text{Material}}$  is the standard deviation of the material, and  $\text{SD}_{\text{PMMA}}$  is the standard deviation of the background.

Low-contrast resolution is related to the ability to discriminate structures with slight differences in attenuation properties. Low-contrast resolution is commonly expressed as the minimum detectable size of an image structure relative to the contrast background. Low contrast was obtained through disc 6, on which 7 ROIs, 5 mm in diameter, were constructed in each polypropylene rod. The polypropylene rods had diameters of 7 mm, 6 mm, 5 mm, 4 mm, 3 mm, 2 mm, and 1 mm, with heights of 10 mm. Another ROI placed on PMMA, with the same dimensions (5 mm) and the same slice, was used to represent the background values. Low-contrast assessment was performed using polypropylene and a PMMA background and calculated using the CNR (Equation 2). Polypropyl-

**Table 2.** Methods automatically defined to select the best image per disc

Disc ID	Disc	Method for disk identification
D2		A 100 mm diameter central ROI of is define and the slice with the highest pixel mean value is selected;
D4		A 5 mm diameter ROI is defined on PTFE considering the positioning coordinates, the highest mean pixel value of this material is selected;
D7		A central square ROI with 40 mm size with the highest standard deviation pixel value is used to select the image;
D6		A central 10 mm diameter ROI is defined and the highest pixel mean value is selected;
D1		A distance of 5 mm from the bottom of phantom;
D5		A central square ROI with 10 mm size with the highest standard deviation pixel value is used to select the image;

ene has subtle differences from PMMA, making this arrangement suitable for representing low-contrast resolution.

The image noise was evaluated from the application of circular ROIs (diameter, 30 mm) corresponding to one-fifth of the phantom diameter (Equation 3). These ROIs were positioned in the center of disc 2. Noise was considered as the standard deviation from the average value in 5 consecutive axial sections and calculated as:

$$\text{Noise} = \left( \frac{\sum_1^5 SD}{5} \right) \times \frac{1}{1000}. \quad (3)$$

The geometric accuracy was obtained from the known values of the distances between the micro-holes, which were measured and compared with known distances (10 mm), both vertically and horizontally.

The spatial resolution was evaluated by the bar pattern (5 lp/cm to 16 lp/cm) located in disc 5. A linear ROI in the center of the bar pattern was plotted, and a graph representing the spatial resolution was constructed.

Image uniformity was evaluated using the pixel intensity measurements obtained from disc 02. ROIs (diameter, 10 mm) were placed around the periphery, and also in the center (1 ROI) of the PMMA. The measurements were made in a transaxial slice and calculated using:

$$\text{Uniformity: } \pm 100 \frac{(Max - Min)}{(Max + Min)}, \quad (4)$$

where *Max* is the maximum mean pixel intensity of the disc 5 ROIs and *Min* is the minimum value of the mean pixel intensity of the ROIs.

The artifacts were measured on disc 7 of the phantom, and the mean pixel value in PMMA was obtained without the presence of metallic objects. The value of the pixel intensity from disc 7 was subtracted from the blank PMMA, and only pixels with a high signal from the metallic artifact were shown. Two ROIs were drawn around the implants, and the mean values of the adjacent exposed

metal objects were obtained. The artifact index was measured as:

$$\text{Artifact}_{Index} = \frac{MP_{ART} + MP_{PMMA}}{MP_{PMMA}}, \quad (5)$$

where  $MP_{ART}$  and  $MP_{PMMA}$  are the mean pixel values in the adjacent area of the rods and PMMA, respectively.

The metallic objects produced higher values than the PMMA; thus, a higher artifact index value was attributed to a greater contribution of the metallic artifacts.

Finally, a report was generated containing the results and an analysis of the information. In addition to quantitative information regarding image quality indicators, exposure parameters, dose area product (DAP), and the next date for quality control tests were also presented.

The results can be exported for further processing as graphical plots. The program can run independently of the operating system and has the possibility to add new functions.

#### Quality control data records and management

The data were automatically exported to Microsoft Excel (.xls), where they were stored in a database and saved in the Portable Document Format (.pdf). In Excel, specific informatics code was developed in Microsoft Office Visual Basic for additional processing of the data and to record the results. This system also informs the user when new tests should be performed.

## Results

The software was tested in 3 CBCT units available on the market, using 7 protocols, as shown in Table 3. The scanners had different configurations (tube potential, voxel size, and product current time) and mode of exposure (high and low dose/resolution).

The software performed automatic measurements and calculations of the SNR, the CNR, image uniformity,

**Table 3.** Cone beam computed tomography (CBCT) phantom acquisition exposure parameters per scanner

CBCT	Protocol	FOV mm	Exposure mode	kVp	mA	Voxel (mm)	mAs
NewTom 5G	N1	180 × 160	Reg	110	1	0.30	2.00
	N2	80 × 80	Hi Reg	110	1	0.15	19.76
	N3	80 × 80	Eco	110	1	0.30	9.60
Cranex 3D	C1	80 × 60	Mini	90	3	0.30	3.5
	C2	80 × 60	Std	90	8	0.30	19.0
Scanora 3D	S1	145 × 75	Std	90	10	0.35	22.5
	S2	60 × 60	Std	90	10	0.20	30.0

Reg: regular time of exposure; Hi Reg: high resolution with regular time of exposure, Eco: low time of exposure, Mini: low dose, Std: standard

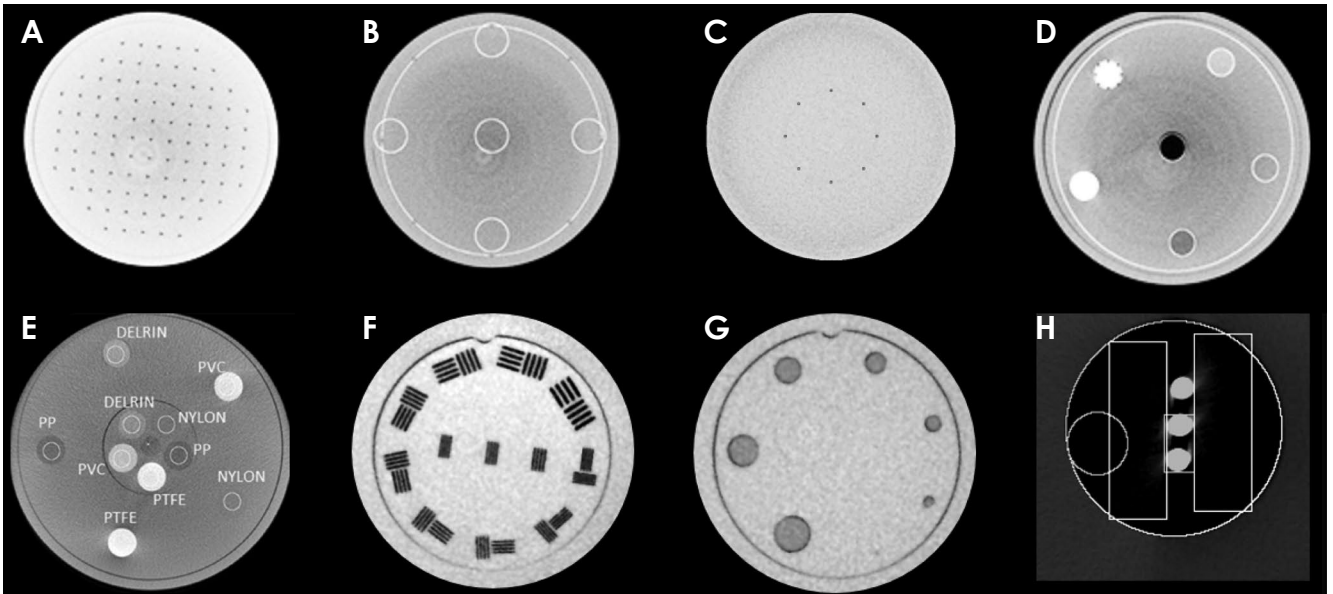


**Fig. 4.** Images obtained in CBCT scanners. A. Disc 1 for geometric accuracy, B. Disc 2 with ROI's positioned to evaluate the image uniformity, C. Disc 2 with a circular ROI ( $\varnothing$  30 mm) in the center, D. Disc 3 with central hole containing air, E. Disc 4 used to evaluate the SNR and CNR in centered and periphery elements, F. Disc 05 with pattern bars, G. Disc 06 to evaluate the low contrast, and H. Disc 7 with three metallic rods and subtracted PMMA background

image noise, geometric accuracy, spatial resolution, low-contrast resolution, and the artifact index. Figure 4 shows the imaging of the phantom and each slice used.

The results obtained through CBCT QA are presented in Table 4. It was possible to observe that the SNR and CNR differed among the scanners and protocols. The highest-density objects (PTFE and PVC) presented higher values of the SNR and CNR, but were more dependent upon the exposure protocol. PP showed a lower SNR value in all protocols, while nylon displayed a lower CNR value. For the Scanora 3D and NewTom 5G, the SNR and CNR values from the centered and peripheral rods were evaluated. The values obtained in NewTom 5G with the N1 protocol did not show any significant differences, and the same behavior was observed in Scanora 3D with the S1 protocol. Regarding noise, the N1 protocol (NewTom 5G) obtained a higher value (6.66) than the other 6 protocols. In contrast, the N2 protocol presented a lower noise level than the other CBCT units.

The image uniformity was also evaluated, and the FOV of  $60 \times 60$  mm showed a significant non-uniform gray value distribution. For the NewTom 5G, the images also showed a non-uniform gray value distribution, mainly with the N1 protocol. In contrast, the N3 and N2 protocols showed a slightly uneven gray value distribution, as did the Cranex 3D. The results of low contrast are shown in Figure 5. The CBCT units were not able to resolve the

1 mm rod.

Geometric accuracy was assessed by measurements (vertical and horizontal) of the distance between 2 points. This test showed that the distances between the micro-holes were smaller than 10 mm.

There were no significant differences in the presence of metal artifacts across the protocols evaluated. The spatial resolutions were obtained and are presented in Figure 6. The first gap represents the visualization of 15 lp/cm, the second of 14 lp/cm and the third of 12 lp/cm. The N2, C2, and S2 protocols allowed the visualization of 15 lp/cm. Other protocols were very strongly influenced by noise and, consequently, low radiation doses.

One of our goals was that the software should be user-friendly and as objective as possible for the user. Therefore, after installation, all results were obtained, presented in a report, and stored in an *.xls* file, as shown in Figure 7.

## Discussion

In the literature, studies have evaluated image quality through different methods including the influence of exposure parameters, or based on a subjective analysis using the visualization of anatomical reference points in anthropomorphic phantoms, skulls, or patient data, which can lead to clinically relevant results.<sup>16</sup> However, this type

**Table 4.** Image analysis results for Cone beam computed tomography scanners and protocols

Protocol	Materials	SNR <sub>C</sub>	Uniformity	Noise	CNR <sub>C</sub>	Artifact	Geometric accuracy		SNR <sub>P</sub>	CNR <sub>P</sub>
							Ver	Hor		
N1	PMMA	3.22								
	PTFE	10.10			2.59				13.02	2.60
	PVC	6.59			1.43				9.62	1.86
	Delrin	4.16	5.09	6.66	0.30	1.05	9.50	9.23	4.49	0.40
	Nylon	3.31			0.12				3.75	0.10
	PP	2.59			0.49				2.97	0.49
	Air	0.78			1.61					
N2	PMMA	34.64							—	—
	PTFE	55.56			7.33				—	—
	PVC	21.13			4.42				—	—
	Delrin	6.82	2.44	1.76	1.05	1.00	9.21	9.65	—	—
	Nylon	4.41			0.03				—	—
	PP	3.27			0.63				—	—
	Air	0.28			7.29				—	—
N3	PMMA	18.90							—	—
	PTFE	23.78			4.42				—	—
	PVC	9.65			2.33				—	—
	Delrin	4.22	1.26	3.54	0.64	1.04	9.84	9.50	—	—
	Nylon	2.93			0.03				—	—
	PP	2.20			0.37				—	—
	Air	0.45			4.65				—	—
C1	PMMA	11.82							—	—
	PTFE	22.85			1.9				—	—
	PVC	11.93			0.23				—	—
	Delrin	5.72	2.35	3.97	1.86	1.03	9.48	9.50	—	—
	Nylon	4.09			2.4				—	—
	PP	3.32			2.71				—	—
	Air	0.71			3.86				—	—
C2	PMMA	8.57							—	—
	PTFE	19.29			1.76				—	—
	PVC	10.90			0.14				—	—
	Delrin	5.34	2.26	4.98	1.40	1.03	9.57	9.28	—	—
	Nylon	3.50			2.09				—	—
	PP	2.58			2.48				—	—
	Air	0.31			3.69				—	—
S1	PMMA	2.40							—	—
	PTFE	12.44			3.00				22.70	4.20
	PVC	6.74			1.73				9.78	2.47
	Delrin	2.94	7.92	3.96	0.28	1.06	9.25	9.95	4.16	0.83
	Nylon	2.34			0.028				2.37	0.29
	PP	1.93			0.27				1.85	0.04
	Air	0.68			1.1				—	—
S2	PMMA	11.17							—	—
	PTFE	17.07			1.93				—	—
	PVC	10.84			0.11				—	—
	Delrin	4.42	7.35	4.11	2.60	1.01	9.73	9.56	—	—
	Nylon	3.19			3.14				—	—
	PP	2.86			3.38				—	—
	Air	0.89			4.29				—	—

SNR<sub>C</sub>: signal to noise ratio in the center, CNR<sub>C</sub>: contrast to noise ratio in the center, SNR<sub>P</sub>: signal to noise ratio in the periphery, CNR<sub>P</sub>: contrast to noise ratio in the periphery, Ver: vertical, Hor: horizontal, PMMA: Polymethyl methacrylate, PTFE: polytetrafluoroethylene, PVC: Polyvinyl chloride, PP: polypropylene



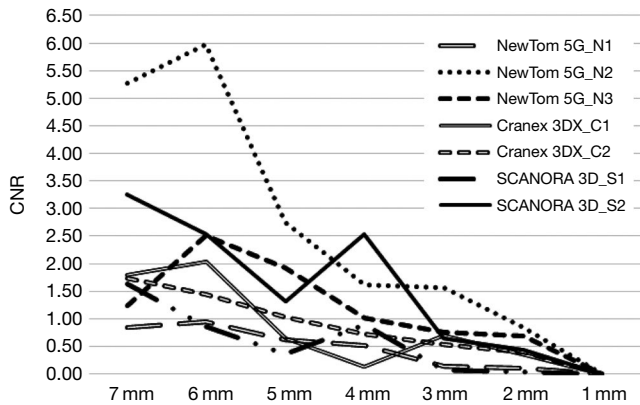


**Fig. 5.** Low contrast evaluation according to the protocol and contrast-to-noise ratio (CNR) in seven rods with diverse diameters

of evaluation is based on the observer's experience and is also dependent upon the monitor quality.<sup>17</sup> CBCT QA, with a standardized method, is extremely important and should be performed frequently. In addition, by performing tests proposed by the manufacturer or regulatory authority, it is possible to detect, for example, deterioration in the accuracy and the difference in contrast between structures over time, indicating that there are problems with the scanner.<sup>18</sup> Presently, applying the recommended guidelines is time-consuming and requires qualified personnel in the health services to perform the tests. In this study, a fast and user-friendly software program was presented, in which any staff member can perform the tests, even an inexperienced user. ImageJ is open-source software and allows one to add, adjust, or implement other functions within the plugin. Since ImageJ is free software, this is an inexpensive method, as it does not require a user license. Bamba et al.<sup>11</sup> considered this approach very useful and encouraged the development of plugins in ImageJ to evaluate image quality in CBCT with phantoms. Donini et al.<sup>19</sup> showed the feasibility of software implemented as a plugin, such as ImageJ, to perform an image check of X-ray based projection radiography, mammography, and angiography/fluorography.

This study presented a new method to evaluate image quality parameters in CBCT. The image uniformity showed different values between CBCT devices in uniformity and in SNR. According to Reeves et al.,<sup>20</sup> there is a lack of gray-level uniformity in CBCT images. These variations could be influenced by the applied scanning parameters. For example, when large voxels are used, the noise tends to be lower. However, maintaining a constant tube potential and increasing the product current time, using smaller voxels, will result in the image being more

uniform. Furthermore, the distribution of gray levels and noise signal may also be related to the amount of mass within the FOV, the use of a wide cone angle (leading to degradation and artifacts), and the size of the reconstructed voxel.<sup>15,21</sup> For the C1 protocol in the Cranex 3DX, even using a higher current exposure time (19 mAs) than the C2 protocol (3.5 mAs), the SNR and uniformity showed only subtle differences. The C2 protocol compensated for the lower mAs by increasing the number of photons owing to the large FOV.

Likewise, an objective evaluation of the effect of downsampling on contrast resolution through calculation of the CNR is encouraged in image quality assessment.<sup>22</sup> The CNR increased as a function of increased tube current time. However, owing to the wide range of voxel sizes used in dental CBCT, it is not possible to compare CNR values from different studies, even if the same phantoms or materials were used.<sup>23</sup>

One of elements that affected the image quality was the presence of metallic artifacts due to high-density objects such as implants. Artifacts are shown as visible structures that do not belong to the object in the image. Thus, artifacts have been argued to be one of the main causes of interference with the diagnostic quality of computed tomography and CBCT.<sup>24,25</sup> Furthermore, this effect could reduce the contrast and obscure structures, thus limiting the anatomical information. The phantom that was used had 3 metallic implants that generated artifacts. The software found the slice with the implants, made 2 rectangular ROIs parallel to the implants, and calculated the artifact index. Even though the results showed no significant differences in the artifact index value, it was possible to evaluate the effect of the adjustment of exposure parameters, such as the increase of the current exposure time or the peak tube potential.<sup>26</sup>

Spatial resolution is an important image quality parameter, especially regarding anatomical details.<sup>27</sup> The N2 protocol showed the best spatial resolution, followed by S2 and C2. This could be related to the use of smaller voxels: the voxels in N2 were 0.15 mm, and 0.2 in S2 mm. However, according to a 2011 study by Pauwels et al.,<sup>15</sup> voxel size alone is a poor predictor of spatial resolution. The variability of the number of line pairs found between the CBCT equipment was not only determined by the spatial resolution of the system, but was also affected by noise and geometrical accuracy.<sup>16</sup> In addition, the spatial resolution of CBCT devices is related to the physical pixel size of the sensor, the reconstruction technique, and other factors.<sup>27</sup>

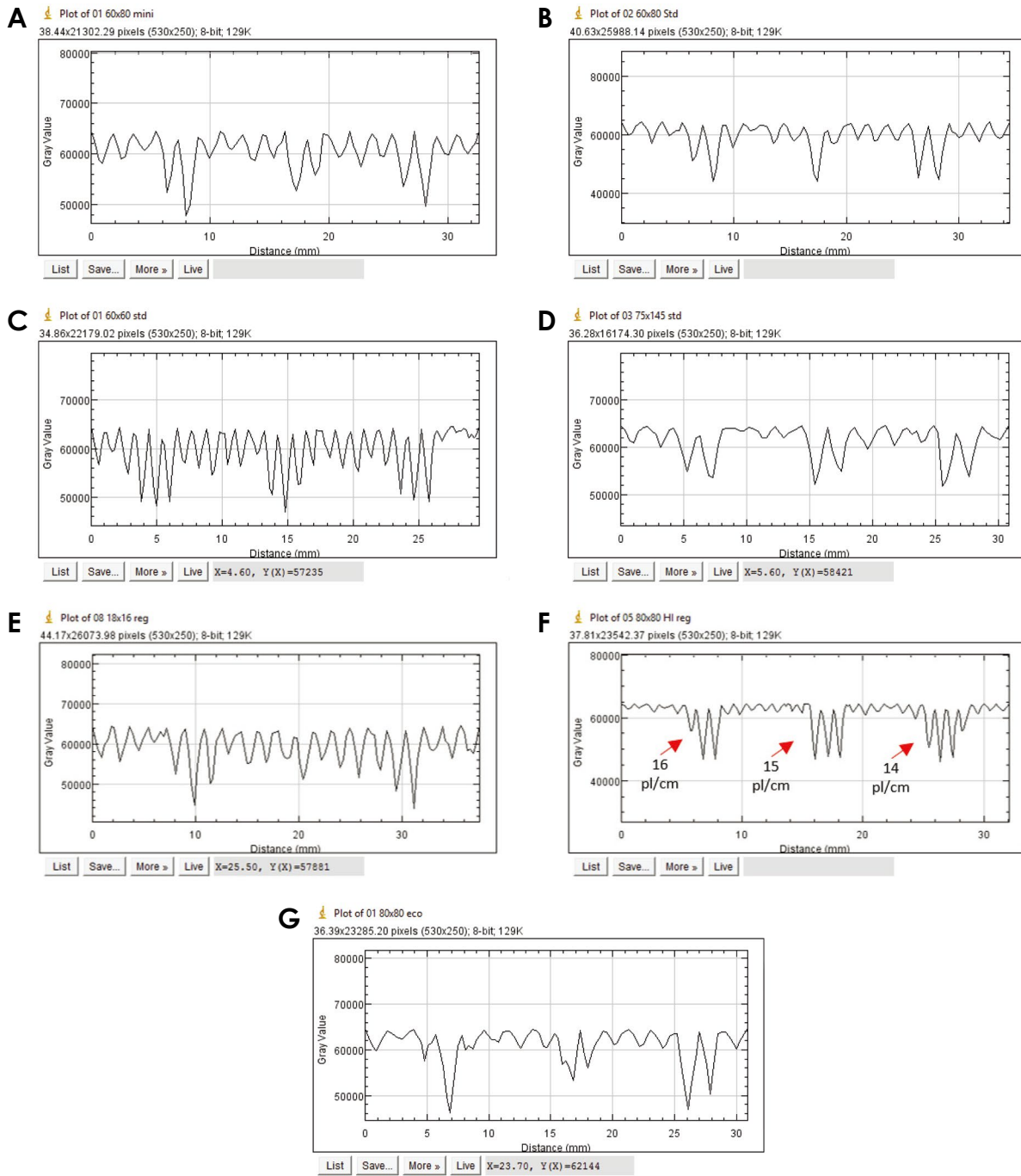


**Fig. 6.** Spatial resolution of CBCT units: A. Cranex 3Dx\_C1, B. Cranex 3Dx\_C2, C. Scanora 3D\_S1, D. Scanora 3D\_S2, E. NewTom 5G\_N1, F. NewTom 5G\_N2, and G. NewTom 5G\_N3.

CBCT is currently exceedingly popular among orthodontists, mainly for craniometric measurements, determining the location of supernumerary and impacted teeth, and orthognathic surgery planning. The accuracy of images has been studied using different scanners,<sup>28</sup> radiographic methods, and 3-dimensional surface-rendered imaging.<sup>29</sup> In this study, all measurements were lower

than the real values (10 mm). These variations may have been influenced by the voxel size and the number of projections.<sup>11,30</sup> Therefore, clinically, variations in distance measurements should be considered, independently of the protocol or CBCT unit.

The low-contrast test showed that the rod with a diameter of 1 mm was not observed in the 3 CBCT units. This

**CBCT**  
Quality Assurance

**MENU** version 1.1

N° 000013 Search n° 000013

Institute: ICS

Technologist: MARCUS Next Test: 10/01/17  
Date: 10/11/2016 29 DAYS  
CBCT: NEW TOM 5G

Add Inf:

**Protocol**

Tube Potential kVp:	120	FOV(H xD):	8X8
Tube current mA:	10	Voxel (mm):	0.2
Product current-time mAs:	45	Time exp.(s):	2
		Arc rotation (°):	360

Checked by: MARCUS

**QUALITY ASSURANCE**

Geometric Accuracy	9.54	Noise	6.63
UNIFORMITY	3.42	Spatial Resolution	15 lp/mm
ARTIFACT INDEX	1.23	Low Contrast	2 mm
		DAP (mGy . cm <sup>2</sup> )	1343.11
CNR		RSR	
AIR	1.61		
PVC	1.43	6.59	
PP	0.49	2.59	
TEFLON	2.59	10.10	
DELIRIN	0.30	4.16	
NYLON	0.12	3.31	

Fig. 7. Data storage system.

suggests that care should be taken in the investigation of structures with low contrast and a small size. Moreover, some rods were influenced by the artifacts yielded by metallic implants, such as in disc 7. However, the device’s contrast resolution was not limited by this factor.

Periodic testing is of utmost importance, both in acceptance testing and to investigate image degradation over time. Our software allows data to be stored in Microsoft Excel (with functions that contain macros to print, save as .pdf, and others), such that performance over time can be monitored, and the user is notified when new tests should be performed. Other advantages relate to the fact that manufacturers or researchers could use this software to test equipment prototypes, as well as to evaluate new image manipulation tools or new reconstruction algorithms. In this study, a new method to improve the quality control of CBCT images was presented. The user is not required to spend any time searching for the image that should be used, consequently leading to faster results and reducing the risk that inappropriate images could be used.

The main objectives of this study were to demonstrate the application of this software and to show its viability for performing image quality control. However, it was not the focus of this study to evaluate the influence of the scanning protocol.

In conclusion, the present study was performed to showcase the development of a new package to evaluate image quality in CBCT. The evaluation of this package showed results that are comparable with the image quality indicators found in the literature. The macro provided a fast, low-cost, and feasible method for analyzing CBCT images. In addition, this program can be feasibly used to perform acceptance testing and to evaluate image quality degradation over time.

### Acknowledgements

The authors thank the Federal Institute of Bahia, Brazil; Oral Radiology, Department of Dentistry and Oral Health, Aarhus University, Denmark; Coimbra Health School and Coimbra School of Engineering (Dr. Fernando Simões and Dr. Paulo Amaro) of Polytechnic Institute of Coimbra, Portugal; Dental Faculty of the Federal University of Bahia for their support in conducting this study; and Dr. Wilson Batista for kindly allow to use of phantom CQ-01-IFBA (intellectual property BR102016 012472-7).

### References

1. Miracle AC, Mukherji SK. Cone beam CT of the head and

- neck, part 2: clinical applications. *AJNR Am J Neuroradiol* 2009; 30: 1285-92.
2. Scarfe WC, Farman AG, Sukovic P. Clinical applications of cone-beam computed tomography in dental practice. *J Can Dent Assoc* 2006; 72: 75-80.
  3. Janner SF, Jeger FB, Lussi A, Bornstein MM. Precision of endodontic working length measurements: a pilot investigation comparing cone-beam computed tomography scanning with standard measurement techniques. *J Endod* 2011; 37: 1046-51.
  4. Plachtovics M, Goczan J, Nagy K. The effect of calibration and detector temperature on the reconstructed cone beam computed tomography image quality: a study for the workflow of the iCAT Classic equipment. *Oral Surg Oral Med Oral Pathol Oral Radiol* 2015; 119: 473-80.
  5. Ludlow JB, Davies-Ludlow LE, Brooks SL, Howerton WB. Dosimetry of 3 CBCT devices for oral and maxillofacial radiology: CB Mercuray, NewTom 3G and i-CAT. *Dentomaxillofac Radiol* 2006; 35: 219-26.
  6. Palomo JM, Rao PS, Hans MG. Influence of CBCT exposure conditions on radiation dose. *Oral Surg Oral Med Oral Pathol Oral Radiol* 2008; 105: 773-82.
  7. Güldner C, Ningo A, Voigt J, Diogo I, Heinrichs J, Weber R, et al. Potential of dosage reduction in cone-beam-computed tomography (CBCT) for radiological diagnostics of the paranasal sinuses. *Eur Arch Otorhinolaryngol* 2013; 270: 1307-15.
  8. Tyndall DA, Rathore S. Cone-beam CT diagnostic applications: caries, periodontal bone assessment, and endodontic applications. *Dent Clin North Am* 2008; 52: 825-41.
  9. SEDENTEXCT Guideline Development Panel. Cone beam CT for dental and maxillofacial radiology. Evidence based guidelines. Luxembourg: European Commission Directorate-General for Energy; 2012.
  10. European Commission. Radiation Protection 136. European guidelines on radiation protection in dental radiology. Luxembourg: Office for Official Publications of the European Commission; 2004.
  11. Bamba J, Araki K, Endo A, Okano T. Image quality assessment of three cone beam CT machines using the SEDENTEXCT CT phantom. *Dentomaxillofac Radiol* 2013; 42: 20120445.
  12. Carter L, Farman AG, Geist J, Scarfe WC, Angelopoulos C, Nair MK, et al. American Academy of Oral and Maxillofacial Radiology executive opinion statement on performing and interpreting diagnostic cone beam computed tomography. *Oral Surg Oral Med Oral Pathol Oral Radiol Endod* 2008; 106: 561-2.
  13. Torgersen GR, Hol C, Moystad A, Hellen-Halme K, Nilsson M. A phantom for simplified image quality control of dental cone beam computed tomography units. *Oral Surg Oral Med Oral Pathol Oral Radiol Endod* 2014; 118: 603-11.
  14. Steiding C, Kolditz D, Kalender WA. A quality assurance framework for the fully automated and objective evaluation of image quality in cone-beam computed tomography. *Med Phys* 2014; 41: 031901.
  15. Pauwels R, Stamatakis H, Manousaridis G, Walker A, Michielsen K, Bosmans H, et al. Development and applicability of a quality control phantom for dental cone-beam CT. *J Appl Clin Med Phys* 2011; 12: 3478.
  16. Pauwels R, Beinsberger J, Stamatakis H, Tsiklakis K, Walker A, Bosmans H, et al. Comparison of spatial and contrast resolution for cone-beam computed tomography scanners. *Oral Surg Oral Med Oral Pathol Oral Radiol Endod* 2012; 114: 127-35.
  17. Suomalainen A, Kiljunen T, Käser Y, Peltola J, Kortensniemi M. Dosimetry and image quality of four dental cone beam computed tomography scanners compared with multislice computed tomography scanners. *Dentomaxillofac Radiol* 2009; 38: 367-78.
  18. Loubele M, Jacobs R, Maes F, Denis K, White S, Coudyzer W, et al. Image quality vs radiation dose of four cone beam computed tomography scanners. *Dentomaxillofac Radiol* 2008; 37: 309-18.
  19. Donini B, Rivetti S, Lanconelli N, Bertolini M. Free software for performing physical analysis of systems for digital radiography and mammography. *Med Phys* 2014; 41: 051903.
  20. Reeves TE, Mah P, McDavid WD. Deriving Hounsfield units using grey levels in cone beam CT: a clinical application. *Dentomaxillofac Radiol* 2012; 41: 500-8.
  21. Bryant JA, Drage NA, Richmond S. Study of the scan uniformity from an i-CAT cone beam computed tomography dental imaging system. *Dentomaxillofac Radiol* 2008; 37: 365-74.
  22. Lukat TD, Perschbacher SE, Pharoah MJ, Lam EW. The effects of voxel size on cone beam computed tomography images of the temporomandibular joints. *Oral Surg Oral Med Oral Pathol Oral Radiol* 2015; 119: 229-37.
  23. Pauwels R, Silkosessak O, Jacobs R, Bogaerts R, Bosmans H, Panmekiate S. A pragmatic approach to determine the optimal kVp in cone beam CT: balancing contrast-to-noise ratio and radiation dose. *Dentomaxillofac Radiol* 2014; 43: 20140059.
  24. Bechara B, Moore W, McMahan C, Noujeim M. Metal artefact reduction with cone beam CT: an in vitro study. *Dentomaxillofac Radiol* 2012; 41: 248-53.
  25. Bechara B, Alex McMahan C, Moore WS, Noujeim M, Teixeira FB, Geha H. Cone beam CT scans with and without artefact reduction in root fracture detection of endodontically treated teeth. *Dentomaxillofac Radiol* 2013; 42: 20120245.
  26. Bechara B, McMahan C, Geha H, Noujeim M. Evaluation of a cone beam CT artefact reduction algorithm. *Dentomaxillofac Radiol* 2012; 41: 422-8.
  27. Brullmann D, Schulze RK. Spatial resolution in CBCT machines for dental/maxillofacial applications-what do we know today? *Dentomaxillofac Radiol* 2015; 44: 20140204.
  28. Suomalainen A, Vehmas T, Kortensniemi M, Robinson S, Peltola J. Accuracy of linear measurements using dental cone beam and conventional multislice computed tomography. *Dentomaxillofac Radiol* 2008; 37: 10-7.
  29. Hassan B, van der Stelt P, Sanderink G. Accuracy of three-dimensional measurements obtained from cone beam computed tomography surface-rendered images for cephalometric analysis: influence of patient scanning position. *Eur J Orthod* 2009; 31: 129-34.
  30. Gribel BF, Gribel MN, Frazão DC, McNamara JA Jr, Manzi FR. Accuracy and reliability of craniometric measurements on lateral cephalometry and 3D measurements on CBCT scans. *Angle Orthod* 2011; 81: 26-35.